Title
Compact FEL-driven inverse compton scattering gamma-ray source

Authors
Placidi, M
Di Mitri, S
Pellegrini, C
et al.

Publication Date
2017-05-01

DOI
10.1016/j.nima.2017.02.072

Peer reviewed

Compact FEL-Driven Inverse Compton Scattering Gamma-Ray Source

M. Placidi [a)], S. Di Mitri [b)], C. Pellegrini [c,d)] and G. Penn [a)]

[a)] Lawrence Berkeley National Laboratory, Berkeley, California 94720, USA

[b)] Elettra - Sincrotrone Trieste S.C.p.A., 34149 Basovizza, Trieste, Italy

[c)] SLAC National Accelerator Laboratory, Menlo Park, California 94025, USA

[d)] University of California, Los Angeles, California 90095, USA

Abstract

Many research and applications areas require photon sources capable of producing gamma-ray beams in the multi-MeV energy range with reasonably high fluxes and compact footprints. Besides industrial, nuclear physics and security applications, a considerable interest comes from the possibility to assess the state of conservation of cultural assets like statues, columns etc., via visualization and analysis techniques using high energy photon beams. Computed Tomography scans, widely adopted in medicine at lower photon energies, presently provide high quality three-dimensional imaging in industry and museums. We explore the feasibility of a compact source of quasi-monochromatic, multi-MeV gamma-rays based on Inverse Compton Scattering (ICS) from a high intensity ultra-violet (UV) beam generated in a free-electron laser by the electron beam itself. This scheme introduces a stronger relationship between the energy of the scattered photons and that of the electron beam, resulting in a device much more compact than a classic ICS for a given scattered energy. The same electron beam is used to produce gamma-rays in the 10-20 MeV range and UV radiation in the 10–15 eV range, in a ~4×22 m^2 footprint system.

1. Introduction

Compact tunable X-ray sources associated with various imaging techniques have been developed and used in a large number of areas ranging from spectroscopy, radiology, medical and biological applications to security, aerospace industry and cultural heritage science. In particular, the field of applications in Geo-archaeology is very wide. It goes from very small archaeological findings like prehistoric teeth and old jewelry, to large artifacts and burial objects wrapped inside soil blocks[†], possibly involving considerable sizes. Depending on the nature and composition of the artifacts inside the soil blocks their tomographic analysis may require very penetrating and high power sources of X-rays to gamma-rays [1–5], in combination with detectors capable of providing good resolution imaging for this type of radiation. Methods of X-ray production presently include Inverse Compton Scattering (ICS) facilities [6] and synchrotron radiation sources from insertion devices in electron storage rings.

Contrast imaging of massive sculptures would profit [7] from radiation sources more powerful than the X-ray Computed Tomography (CT) industrial instruments operating in the 450 keV range. In fact, the efficacy of transmission imaging techniques like radiography and tomography depends on the attenuation processes occurring within the object to be imaged. The Beer-Lambert law [8] characterizes this attenuation through a transmission function $T=\exp(-\tau\rho\mu)$, involving the cross section of physical processes such as photoelectric absorption, Compton scattering and pair production. Here τ is the thickness of the sample, ρ is the mass density and μ is the mass attenuation coefficient, which depends upon both the photon energy and the sample composition [9]. Transmission data are given in Table 1 for 20 MeV gamma-rays passing through a 10 cm thickness of different materials of interest to cultural heritage studies. For many of them the transmission is large.

Table 1. Transmission of 20-MeV gamma-rays through a τ=10-cm thickness of different materials.

Sample	Z	ρ [g/cm^3]	μ [10^{-2} cm^2/g]	T [%]
Al	13	2.72	2.17	55.4
Fe	26	7.87	3.22	8.0
Cu	29	8.96	3.41	4.7
Ag	47	10.49	4.61	0.79
Au	79	19.32	6.14	7.1×10^{-4}
Pb	82	11.35	6.21	8.7×10^{-4}
Bone	-	1.92	2.07	67.2
Concrete	-	2.30	3.44	45.3
Calcite	-	2.71	2.28	53.9

[†] Soil blocks resulting from archaeological excavations may contain different kinds of artifacts of interest in cultural heritage.

In this paper we discuss a system, based on ICS, to produce gamma rays up to 20 MeV, minimizing the electron beam energy and total footprint. In the proposed scheme, the electron beam interacts with its own radiation emitted in an ultra-violet (UV) Free Electron Laser (FEL), as shown in Fig. 1, making UV and gamma rays available from the same system.

It was mentioned above that a diversity of applications can be found in very different research fields, see for example [10] and references therein. Specific case studies can be identified, for example, on the basis of the energy content of the scattered light. At low photon energy (up to few MeV), the aforementioned contrast imaging of massive objects in Geo-archeology [7] would greatly benefit from such an intense and compact source, and this was actually the driving case of this work. At photon energies in the 1–10 MeV range, photons propagating though dense materials prompt nuclear reactions, generating e.g. alpha particles and neutrons, which can be easily identified and used for separating isotopes [11]. At photon energies higher than 10 MeV, the proposed scheme would approach the specifications for an elastic photon-photon scattering source for frontier experiments in QED [12]. Even if all these examples were equivalently considered in the presence of an external laser, it is undoubtedly demonstrated below that a higher electron beam energy would be required at the interaction point, for the same output photon energy, and therefore a longer, more expensive electron linear accelerator. Moreover, as a by-product of the proposed scheme, a naturally synchronized UV beam with large fraction of coherent photons, and at 100 fs duration level would be provided by the FEL, which is ideal for pump-probe experiments.

2. Energy scaling for FEL-ICS radiation

In an ICS process, a relativistic electron transfers a fraction of its energy to an incoming photon, scattered in the electron direction of flight, with a Doppler upshifted frequency. The wavelength of the scattered radiation is

$$E_s = a_C \gamma^2 \hbar\omega_{ph}, \tag{1}$$

where $\hbar\omega_{ph} = E_L$ is the incoming laser photon energy, γ the Lorentz factor and

$$a_C \approx \frac{2(1+\cos\varphi)}{1+(\gamma\theta)^2} \le 4. \tag{2}$$

Here φ is the collision angle and θ the observation angle. The upper limit corresponds to on-axis radiation in head-on collisions. The scattered photon energy exhibits a quadratic dependence on the electron energy.

With our FEL-ICS scheme, we introduce a stronger γ-dependence by making the relativistic electron beam interact with its own UV radiation produced in an FEL [13]. The on-axis FEL radiation wavelength is related to the axial electron velocity β_z and the undulator period λ_u as [14]:

$$\lambda_r = \lambda_u \frac{1-\beta_z}{\beta_z} \approx \frac{\lambda_u}{2\gamma^2}(1+a_u^2). \tag{3}$$

Here $a_u = K_u = eB_0\lambda_u / 2\pi m_e c = 93.4 B_0 \lambda_u$ is the helical undulator parameter ($a_u = K_u/\sqrt{2}$ for a planar-polarized undulator), B_0 the undulator central magnetic field, e the electron charge. In terms of the electron energy the energy of the FEL photons is:

$$E_r \equiv \frac{hc}{\lambda_r} = hc\, a_{FEL} \frac{\gamma^2}{\lambda_u}, \tag{4}$$

where we define $a_{FEL} = 2/(1+a_u^2)$ for on axis undulator radiation.

When the FEL photon energy (4) replaces that from the laser in Eq. (1), i.e., $\hbar\omega_{ph} = E_r$, the scattered photon energy reads:

$$E_s = a_C \gamma^2 E_r = a_C a_{FEL} hc \frac{\gamma^4}{\lambda_u}. \tag{1'}$$

The scattering efficiency, defined as the fraction of the electron energy transferred to the scattered photons, reads

$$\eta \equiv \frac{E_s}{E} = a_C\, a_{FEL} \frac{\lambda_c}{\lambda_u} \gamma^3, \tag{5}$$

having introduced the Compton wavelength $\lambda_c = hc/m_e c^2 = 2.4\text{x}10^{-12}$ m. While the scattering efficiency in the ICS case scales linearly with beam energy, the cubic energy dependence in Eq. (5) provides compactness to the system, as lower electron

energy is required for a given photon energy. Additional flexibility in the UV energy and thus in the FEL-ICS radiation is available as they are tunable via the undulator parameter K_u, typically ranging from 1 to 5 in an out-of-vacuum APPLE-II type device [15] or Delta undulator [16].

The collision angle φ at the Interaction Point (Fig. 1) is different from zero to allow room for optical components. Some reduction on the scattering efficiency via the impact parameter a_C and the length of the collision overlap is acceptable for an interaction angle up to $\varphi=25^0$ which will be considered in the FEL-ICS baseline design.

3. A baseline FEL-ICS system and its components

3.1. – Description of the baseline design

A single-pass conceptual layout providing a strong source of multi-MeV photons is shown in Fig. 1. The main characteristics of the system are summarized in Table 2 and discussed in the following sections. Trains of electron bunches from an X-Band Linac are focused at the IP where they collide with FEL radiation produced by earlier bunches. A return arc guides the electrons into an FEL undulator. The return arc is designed to act as a bunch length compressor [17,18], raising the electron bunch peak current from 35 A to 500 A for an improved FEL performance. The FEL operates in the high-gain SASE regime [14,19] and is long enough to reach saturation. The emerging UV radiation is focused at the IP, where high-energy gamma-rays are produced via Compton interaction with the trailing bunches. The 180° original arc deflection from Ref. [17] is extended to 205° to produce collisions at a 25° interaction angle.

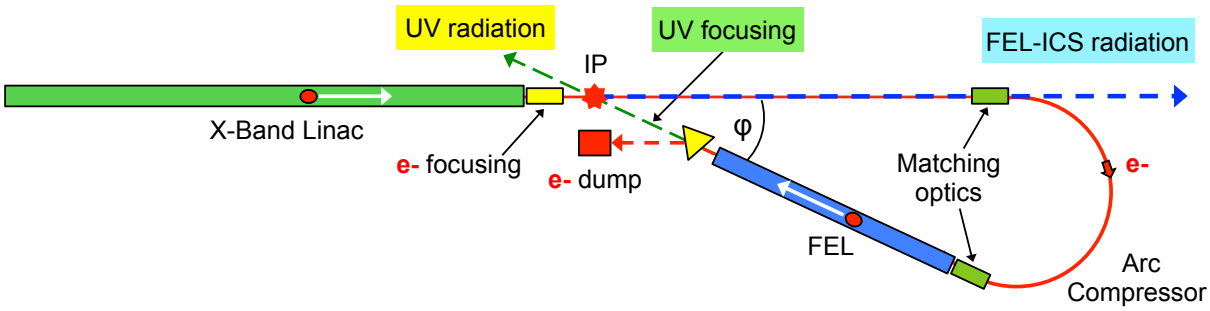

Fig. 1. FEL-ICS scheme with an electron beam return arc. Two photon energies are simultaneously available to experiments. Quadrupole triplets provide overlap control at the IP and beam properties matching for arc and undulator. The return arc provides longitudinal bunch compression for improved FEL performance. The system footprint is about 4×22 m^2.

The low value of the Thomson cross section preserves the electron bunch quality for the FEL and allows subsequent use of the UV radiation for additional applications. The large FEL power compensates for the low Thomson cross-section. The electron bunches and UV radiation are focused to similar transverse spot sizes at the IP to optimize the scattered flux. The electron focusing, bunch compression, and UV optics are all crucial for providing the desired compactness and gamma-ray flux. The short undulator length allowed by bunch compression makes the footprint of the single-pass scheme essentially determined by the Linac and the return arc. An arc compressor length of about 6.5 m and the associated matching optics leave about 2.5 m for the UV focusing drift downstream the undulator. For a 10 m Linac length, the system footprint is ~ 4×22 m^2.

Other FEL-based ICS schemes, using an optical cavity to generate collisions between the FEL photons and the electron beam, exist [6] or have been proposed [20]. Our scheme removes this requirement and is not limited to FEL wavelengths for which highly reflective mirrors at normal incidence are available, taking full advantage of the scaling law of Eq. (1′).

3.2. – The linear accelerating structure

We consider a linac operating at room temperature in the original spirit of keeping the photon source within cost-effective limits. High-gradient X-Band technology [21], both for the photo-injector and the accelerating structure, is used to make the system compact. The linac is run at 1 kHz and the average power need to operate it is minimized by using X-band frequency, 11.4–12.0 GHz . Warm X-Band RF technology operating at 1 kHz with a 35 MV/m gradient has been considered in [22,23] and is adopted in our design. Such gradient is considerably lower than the 100 MV/m reached at the CTF [24] in laboratory operating conditions, at repetition rates below 100 Hz. A beam energy of 300 MeV can be achieved in a 10 m long footprint. Each of the 1 μs long RF pulses can host a train of 100 electron bunches 10 ns apart, for a bunch repetition rate of 100 kHz.. A 300 pC bunch charge gives an average beam current of about 30 μA, and a 9 kW average beam power.

An X-Band photo-injector running with beam loading at low repetition rates has been built and commissioned at the X-Band Test Area (XTA) at SLAC, providing good beam quality [25].

3.3. – Return arc compressor

The return arc compressor gives a 205° beam deflection via a modified double-bend achromatic cell magnetic structure characterized by a 3.58 Tm integrated bending field at E=300 MeV. The 6.5 m central arc trajectory length has an average radius R_{ARC}=1.82 m. It yields a bunch length compression factor C≈15 for 300 pC bunches, while limiting the growth of the transverse projected normalized emittances – here weakly affected by the emission of coherent synchrotron radiation (CSR) – to about 0.3 μm. The outgoing bunch has 0.5 kA peak current, 1 μm normalized projected emittances and ~0.2% correlated rms energy spread. Particle tracking indicates that CSR emission in the arc dipoles leads to some modulation in the bunch current profile and energy distribution. Nevertheless, the final relative slice energy spread remains about one order of magnitude lower than the FEL parameter threshold, and no relevant impact on the FEL performance is anticipated. The bunch final peak current of 0.5 kA is important to obtain high average FEL photon flux and reduce the undulator gain length.

Table 2. Baseline parameter list for the FEL-ICS with return arc compressor.

System	Value	Unit
Linac		
Electron Beam Energy	300	MeV
Photo-Injector RF Frequency (X-Band)	11.4-12.0	GHz
Linac RF Frequency (X-Band)	11.4-12.0	GHz
Linac Accelerating Gradient	35	MV/m
Linac Length	~10	m
Bunch Charge	300	pC
Initial Bunch Duration, rms	2.5	ps
Initial Bunch Peak Current	35	A
Initial Normalized Emittance (x,y), rms	0.7, 0.7	mm mrad
Train Repetition Rate	1	kHz
Number of Bunches per Train	100	
Average Beam Current	30	μA
Beam Power to Dump	9	kW
Return Arc Compressor		
Magnetic Cell Type	DBA-like	
Arc Length	6.5	m
Compression Factor	15	
Final Peak Current	500	A
Final Normalized Projected Emittance (x,y), rms	1.0, 1.0	mm mrad
Final Correlated Relative Energy Spread	0.2	%
Final Uncorrelated Relative Energy Spread	0.02	%
Free Electron Laser		
Undulator Magnetic Structure	Helical	
Undulator Peak Field	0.86	T
Undulator Period Length	20	mm
Undulator Total Length	~5	m
Undulator Parameter	1.6	
FEL Wavelength	103	nm
FEL Parameter	5.5×10^{-3}	
FEL Gain Length	0.22	m
FEL Peak Saturation Power	0.77	GW
UV Peak Flux	4×10^{26}	photons/s
FEL Duty Factor	6×10^{-8}	
UV Average Power	46	W
UV Average Flux	2×10^{19}	photons/s
UV Focusing Drift	2.5	m
UV Coherent Angle	0.16	mrad
UV Coherent Radius	0.052	mm
System footprint	~4×22	m^2

3.4. – The UV FEL

After bunch length compression the beam is injected into the undulator. In the 1-D approximation the FEL gain length is given in terms of the 'FEL parameter' [11], ρ_{FEL}, by

$$L_G = \frac{\lambda_u}{4\pi\sqrt{3}\rho_{FEL}} \quad . \tag{6}$$

The radiation bandwidth and the ratio of saturation power to electron beam power scale linearly with the FEL parameter [11]. In this example, a helical undulator is used to maximize the output power, reduce the gain length and provide transverse focusing. A compact design based on Permanent Magnet technology [15,26] can provide the desired field amplitude, such as B_0=0.86 T at λ_u=20 mm, and eventually an undulator parameter a_u=1.60. A ~5 m long undulator allows the FEL to reach saturation at the fundamental wavelength of 103 nm (12 eV photon energy). The analytical evaluation of the undulator length needed to reach saturation is shown in Fig. 2 as a function of the beam peak current, along with the final average gamma-ray photon flux. With the undulator and electron beam parameters in Table 2, the FEL parameter is about 5.5×10^{-3}, the gain length 0.22 m and the FEL peak power at saturation 0.77 GW. The corresponding photon peak rate is 4×10^{26} UV ph/s.

3.5. – Focusing and tuning at the IP

Bunch length compression and UV optics are crucial for providing a high gamma-ray flux and a reduced system footprint. The UV radiation is focused to optimize the gamma rays production rate by matching the rms size of the electron and photon beams at the IP. The UV optical focusing system uses a single toroidal mirror operating at grazing incidence [27] to compensate the FEL photon beam divergence and produce a 15 μm vertical, 60 μm horizontal photon sizea at the IP, via a demagnification factor of about 4 in the vertical plane and 1 in the horizontal plane for the photon beam dimension at the undulator exit (Table 2) . A bare silicon surface has ~97% reflectivity at 12 eV and 2° grazing incidence. A quadrupole triplet at the end of the linac controls the electron beam sizes to match those of the UV beam .

The transverse matching of the electron and photon beams increases the scattered photon flux by over an order of magnitude compared to a case with no UV focusing. While the UV FEL pulse in the SASE regime has an rms duration comparable to that of the electron bunch after compression, approximately 0.16 ps, the electron bunch at the IP is still uncompressed and has a parabolic current profile with an rms duration of 2.5 ps (Table 2).

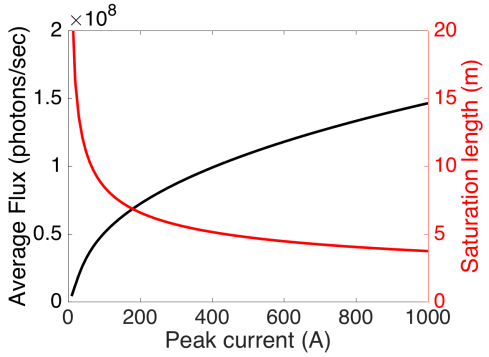

Fig. 2. FEL-ICS performance in terms of average scattered photon flux and FEL saturation length vs. the electron bunch peak current, for an undulator period length λ_u=20 mm.

Being the UV focusing at the IP critically important for the scattered photon beam properties, the pointing stability of the FEL output pulse needs major attention. By virtue of the demagnification factor 4 at the IP for the vertical plane, the FEL pulse rms transverse sizes are 60 μm × 60 μm at the exit of the undulator. If a tolerance on the shot-to-shot variation of the FEL pulse position as large as 1/5 of the rms size is considered, the FEL trajectory has to be controlled at the level of ~10 μm in both planes. This is basically the tolerance on the electron beam trajectory in the undulator. For a minimum betatron function of approximately 2.5 m along the undulator, control of the electron beam angular divergence has to be at the level of ~10 μm /2.5 m = 4 μrad. State-of-the-art SASE FELs in single pass facilities feature < 5 μm, < 1 μrad rms electron trajectory jitter by adopting < 2 μm resolution RF cavity beam position monitors [28]. The unavoidable residual jitter is typically dominated by RF jitter sources in the accelerator that, for the aforementioned ranges of fluctuations, stay at the rms level of 0.1% for the peak voltage, and to 0.1 deg (from S-band to X-band) for the phase [29]. In summary, the proposed FEL-ICS scheme requires a good beam control largely feasible with the presently available technology.

3.6. – Electron beam dump

The 9 kW average electron beam power is spent in a dump (see Fig.1). The electron beam transverse dimensions at this location are larger than 0.1 mm rms in both planes and the single pulse energy density is ≤ 0.17 J/mm^2/pulse. A 0.5 m long cylindrical dump, made of an inner core of Graphite surrounded by Aluminum, would ensure >99% energy absorption efficiency with negligible production of isotopes.

4. Beam temporal structures and event rate

The beam temporal structure consists of bunch trains of length τ_t repeating at the RF pulse rate k_t. Each train contains k_b bunches with a time separation multiple of the gun bucket separation τ_G

$$\tau_b = \tau_t / k_b \equiv m\tau_G \,. \tag{7}$$

The leading bunches in each train do not contribute to the ICS process as they need to fill the loop of Fig. 1 before radiating in the undulator and initiate the scattering process. If N_{loop} is the number of bunches uniformly filling the loop length $L_{loop}=c\tau_{loop}$, the number of bunches in each train actually interacting in the FEL-ICS scheme is:

$$k_{bx} = k_b - N_{loop} = k_b(1 - \tau_{loop}/\tau_t) \tag{8}$$

and the event rate for the FEL-ICS process (in photons per second) can be written as:

$$\dot{N}_{ph}^{ICS} = \frac{\sigma_T}{e\,A(\varphi)} I_L N_{ph}^U (1 - \tau_{loop}/\tau_t) \,. \tag{9}$$

Here $\sigma_T = 0.665\times10^{-24}$ cm^2 is the Thomson cross section, $I_L=k_t\,k_b\,q_b$ the average linac current and N_{ph}^U the number of UV photons per FEL pulse. The expression for the interaction area $A(\varphi)$ for Gaussian bunches colliding at an angle φ in the horizontal plane is

$$A(\varphi) = 2\pi\,\Sigma_y \sqrt{\Sigma_x^2 + \Sigma_z^2 \tan^2(\varphi/2)} \tag{10}$$

where the convoluted transverse bunch sizes are $\Sigma_s = \sqrt{\sigma_{s1}^2 + \sigma_{s2}^2}$ $(s = x, y, z)$ and can be optimized as discussed before.

The synchronism condition associated to the loop length L_{loop} and the bucket separation (Eq.7)

$$\tau_{loop} \equiv \frac{L_{loop}}{c} = q\,\tau_b \qquad (q\text{=integer}) \tag{11}$$

is fulfilled, for a given interaction angle φ, by a proper design of the arc length.

For the footprint geometry sketched in Fig. 1, and the electron beam and undulator parameters listed in Table 2, there are 90 interacting electron bunches per train and the interaction rate at the IP is 90 kHz. The characteristics of the photon and electron colliding beams, and of the scattered gamma-rays are summarized in Table 3. The average gamma-ray photon flux and the undulator saturation length are shown as a function of the beam peak current in Fig. 2. At our design value of 500 A we have 1.1×10^8 ph/s and 5.0 m respectively. The ideal minimum bandwidth for the gamma-rays is 0.9%, determined by a combination of the projected energy spread of the electron bunch, the SASE FEL bandwidth and the angular spread of the electrons. The average scattered photon energy is half of the maximum photon energy, and the scattered intensity on axis is taken to be the total flux divided by a solid angle of $2\pi/3\gamma^2$ [30].

5. Upgrade options

A higher average photon flux is certainly appreciated in experiments that rely on statistics [31] such as those cited in the Introduction as case studies as well as experiments implementing ultrafast dynamics and spectroscopy for the physics of matter at molecular scale. The average photon flux can be made larger at the expense of increasing the complexity of the device, in particular by requiring cryogenic cooling. Superconducting L-Band accelerating structures with frequencies of 1.3 or 1.5 GHz, have been designed for multiple accelerator facilities. Peak gradients are comparable to that of S-Band structures, in the range of 10-20 MV/m, and with quality factor Q > 10^{10} may be run in CW mode. A single 8 m cryomodule can yield ~120 MeV energy gain.

The LCLS-II design [32] has a nominal average current of 20 μA, with a technical limit of 300 μA. With no beam slowing or energy recovery, the main constraint is on the beam dump, which for a 4 GeV beam would need to accept up to 1.2 MW.

Table 3. Beam parameter list at the Interaction Point.

Parameter	Value	Unit
Electron Beam Energy	300	MeV
Bunch Charge	300	pC
Bunch Duration, rms	2.5	ps
Bunch Peak Current	35	A
UV Photon Energy	12.0	eV
UV Peak Flux	2×10^{19}	photons/s
UV Duration, rms	0.16	ps
UV and e- rms beam sizes at IP (x / y)	60 / 15	μm
Interaction Angle	25	deg
Interacting e- Bunches per Train	90	
Interaction Rate	90	kHz
ICS Duty Factor	7.7×10^{-7}	
Scattered Photon Maximum Energy	~16	MeV
Scattered Photon Average Flux	1.1×10^{8}	photons/s
Scattered Photon Average Power	0.14	mW
Scattered Photon Average Intensity	1.8×10^{7}	photons/s/mrad^2
Scattered Photon Peak Flux	1.4×10^{14}	photons/s
Scattered Photon Peak Power	1.8×10^{5}	mW
Scattered Photon Peak Intensity	2.3×10^{13}	photons/s/mrad^2

For a 300 MeV beam energy, a 500 kW beam power at the beam dump would allow an average Linac current of 1.7 mA, corresponding to an increase by a factor ~50 in the total photon flux compared to that evaluated at room temperature operation. The use of energy recovery, such as at the Cornell ERL [33], could allow 100 mA average current but requires a large R&D effort in cavity design and feedback systems. However, significantly more than 1 mA may be achievable using already engineered systems.

The benefits of using SC undulators are not as dramatic as those of SC acceleration. However, by allowing a higher undulator parameter at shorter periods, SC undulators can be used to reduce the beam energy, increase the scattered photon energy, and/or reducing the undulator length. Any improvement in the photon flux will be modest at best.

Finally, seeding the FEL process would improve stability and shorten the required undulator length. It could be achieved either with an external source or through regenerative amplification [34] by sending a small fraction of the output FEL radiation back into the undulator. However, a further reduction of the undulator length would add limited compactness to the system footprint, mainly determined by the return arc length.

6. Summary

Nearly monochromatic multi-MeV gamma-ray beams can find applications in industry and security fields, where their characteristics can play an important role in the analysis of materials and the detection of illegal specimens. In the Geo-archaeology and cultural heritage fields, X-ray Computed Tomography (XCT) techniques [3-5,7], presently adopted for the visualization and analysis of archaeological artifacts contained in soil blocks of limited dimensions (~0.1 m^3), can benefit from the availability of gamma-ray beams in the tens of MeV range to extend the present fields of application. We have demonstrated that by interacting with its own FEL radiation through an Inverse Compton Scattering process, a relatively low energy electron beam can simultaneously produce UV photons in the 10 to 12 eV range, and high-energy gamma-rays in the 6-16 MeV range. These photon beams can be used for Cultural Heritage, Nuclear Physics and UV science.

In the proposed FEL-ICS setup the electron beam interacts with photons generated in an undulator by the electron beam itself. For a given gamma-ray energy the footprint of the setup is reduced, as compared to laser-based ICS facilities, since the energy of the scattered gamma-rays scales with the fourth power of the electron energy. As an example, gamma-rays in the 16 MeV range can be produced with a ~300 MeV electron beam as compared to the ~700 MeV required in a conventional ICS system. Tunability is provided via the undulator field parameter. A compact ~5 m long undulator is sufficient to simultaneously produce an average UV flux of ~2×10^{19} ph/s and a high-energy gamma ray flux in excess of 1×10^{8} ph/s,

within a system footprint of about 4×22 m^2. The scheme can be considered as an alternative to neutrons for the analysis of soil blocks of a certain volume containing archaeological findings like prehistoric teeth and old jewelry in the Geoarchaeology and Cultural Asset field. Moreover, it offers options for a wide range of multi-MeV photons applications in the Industry and Security environments. Superconducting L-Band accelerating structures can increase the average Linac current and the outgoing radiation flux by a factor of 50.

Acknowledgements

One of the authors (MP) wishes to acknowledge initial exchanges with F. Casali and F. Boscherini (Bologna University) with whom he shared the interest for high-energy photon sources devoted to analysis and preservation of Cultural Heritage. He is also indebted to A. Hofmann, M. Zolotorev, W. Leemans, J. Byrd, E. Esarey, C. Schroeder, C. Geddes, M. Cornacchia and F. Villa for enlightening discussions on the feasibility and the scientific validity of the proposal, and to M. Sticco for his help with graphics. We acknowledge valuable contributions from G. D'Auria, L. Doolittle and F. Sannibale on Linac technical aspects and from D. Cocco for a feasibility estimate of a UV focusing system. We also thank A. Ratti for encouraging and supporting this study. This publication was funded by the Accelerators Group of Elettra Sincrotrone Trieste and by the Director, Office of Science, of the U.S. Department of Energy under Contract No. DE-AC02-05CH1123.

References

[1] A. Olivo and E. Castelli, "*X-ray phase contrast imaging: From synchrotrons to conventional sources*", Rivista del Nuovo Cimento, Vol. 37, N. 9 (2014) 467-508, doi:10.1393/ncr/i2014-10104-8.

[2] K. Yamada *et al., "A trial for fine and low-dose imaging of biological specimens using quasi-monochromatic laser-Compton X-rays",* Nucl. Instr. Meth. A **608** (2009) S7-S10, doi:10.1016/j.nima.2009.05.157.

[3] J. Stelzner *et al., "The application of 3D computed tomography with X-rays and neutrons to visualize archaeological objects in blocks of soil"*, Studies in Conservation **55** (2013) 95-106, doi:10.1179/sic.2010.55.2.95.

[4] F. Casali, "*X-ray and neutron digital radiography and computed tomography for cultural heritage*", Physical Techniques in the Study of Art, Archaeology and Cultural Heritage, Volume I, ed. D. Bradley and D. Creagh, Elsevier, Amsterdam (2006) 41-123, doi:10.1016/S1871-1731(06)80003-5.

[5] A. Re *et al.,* "*X-ray tomography of a soil block: a useful tool for the restoration of archaeological finds",* Heritage Science **3** (2015) 4, doi:10.1186/s40494-015-0033-6.

[6] H. R. Weller *et al*., "*Research opportunities at the upgraded HIγS facility*", Progress in Particle and Nuclear Physics **62** (2009) 257–303, doi:10.1016/j.ppnp.2008.07.001.

[7] F. Casali *et al., "X-ray computed tomography for damage assessment of cultural heritage assets",* Proc. International Conference on Protection of Historical Buildings (PROHITECH 09), Mazzolani (ed), (2009) 847-851, Taylor & Francis Group, London, ISBN 978-0-415-55803-7.

[8] A. Beer "Bestimmung der Absorption des rothen Lichts in farbigen Flüssigkeiten" (Determination of the absorption of red light in colored liquids), *Annalen der Physik und Chemie*, vol. 162, pp. 78–88, (1852), doi:10.1002/andp.18521620505.

[9] S. M. Seltzer, "Calculation of Photon Mass Energy-Transfer and Mass Energy-Absorption Coefficients", Radiation Research 136 (1993) 147-170; cf. Table 4 of NIST data at https://www.nist.gov/pml/x-ray-mass-attenuation-coefficients and online absorption calculator at http://webdocs.gsi.de/~stoe_exp/web_programs/x_ray_absorption/index.php.

[10] G. Sarri et al., "*Ultrahigh Brilliance Multi-MeV γ-Ray Beams from Nonlinear Relativistic Thomson Scattering*", PRL 113, 224801 (2014). DOI: https://doi.org/10.1103/PhysRevLett.113.224801

[11] C. P. J. Barty, "*Nuclear photonics with laser-based gamma rays*", *SPIE Opt. Optoelectron*. Paper 8080B-30 (2011). doi: 10. 1117/2. 1201110.003681.

[12] D. Micieli et al., PRST-AB 19, 093401 (2016).

[13] H. Motz, W. Thon and R.N. Whitehurst, "*Experiments on Radiation by Fast Electron Beams*", J. Appl. Phys. **24**, No. 7, (1953) 826, doi:10.1063/1.1721389.

[14] C. Pellegrini, A. Marinelli and S. Reiche, "*The physics of free-electron lasers*", Reviews of Modern Physics **88** (2016) 015006, doi:10.1103/RevModPhys.88.015006.

[15] A. B. Temnykh, "*Delta undulator for Cornell energy recovery linac*", Phys. Rev. ST Accel. Beams 11 (2008) 120702, doi:10.1103/PhysRevSTAB.11.120702.

[16] S. Sasaki, "Analyses for a planar variably-polarizing undulator", Nucl. Instr. Meth. A **347** (1994) 83-86, doi:10.1016/0168-9002(94)91859-7.

[17] S. Di Mitri and M. Cornacchia, "*Transverse emittance-preserving arc compressor for high-brightness electron beam-based light sources and colliders",* EPL **109** (2015) 62002, doi:10.1209/0295-5075/109/62002.

[18] S. Di Mitri, "*Feasibility study of a periodic arc compressor in the presence of coherent synchrotron radiation"* Nucl. Instr. Meth. A 806 (2015) 184-192, doi:10.1016/j.nima.2015.10.015.

[19] R. Bonifacio, C. Pellegrini and L. M. Narducci, "*Collective instabilities and high-gain regime in a free electron laser*", Opt. Commun. **50** (1984) 373, doi:10.1016/0030-4018(84)90105-6.
[20] B. E. Carlsten *et al*., "*High repetition-rate inverse Compton scattering x-ray source driven by a free- electron laser*", J. Phys. B 47 (2014) 234012, doi:10.1088/0953-4075/47/23/234012.
[21] G. D'Auria, "*Application of X-Band Linacs",* Proc. LINAC2012, Tel-Aviv, Israel (2012) 724-728, ISBN 978-3-95450-122-9.
[22] C. Christou, "*X-band linac technology for a high repetition rate light source*", Nucl. Instr. Meth. A **657** (2011) 13, doi:10.1016/j.nima.2011.06.050.
[23] R. Bartolini, "*Beam dynamics optimisation of an X-band Linac driven soft X-ray FEL*", Nucl. Instr. Meth. A **657** (2011) 177, doi:10.1016/j.nima.2011.06.046.
[24] W. Wuensch, HG2012 Workshop, 18-20 April 2012, KEK, Tsukuba, Japan.
[25] C. Limborg-Deprey *et al., "Achieved Performance of an All X-Band Photo-Injector*", Proc. IPAC2016, Busan, Korea (2016) 4253, ISBN 978-3-95450-147-2.
[26] H.-D. Nuhn *et al*., "*Commissioning of the Delta Polarizing Undulator at LCLS*", Proc. FEL2015, Daejeon, Korea (2015) 757-763, ISBN 978-3-95450-134-2.
[27] D. Cocco, private communication.
[28] P. Frisch et al., in Proc. of Intern. FEL Conf., THB04, Basel, Switzerland (2014).
[29] P. Craievich et al. PRST-AB 16, 090401 (2013).
[30] D. Fargion, R.V. Konoplich and A. Salis, "*Inverse compton scattering on laser beam and monochromatic isotropic radiation*", Z. Phys. C **74** (1997) 571—576, doi:10.1007/s002880050420.
[31] W. Graves, "*Compact x-ray source based on burst-mode inverse Compton scattering at 100 kHz*", PRST-AB **17, 120701 (2014)**],
[32] LCLS-II Design Study Group, "*LCLS-II conceptual design report*", Report LCLSII-1.1-DR-0001-R0, SLAC, January 2014.
[33] M. Liepe, D. Hartill, G. Hoffstaetter, S. Posen, and V. Veshcherevich, "*Experience with the Cornell ERL injector srf cryomodule during high beam current operation*", Proc. IPAC2011, San Sebastian, Spain, (2011) 35-37.
[34] D. C. Nguyen et al., "First lasing of the regenerative amplfier FEL", Nucl. Instr. Meth. A **429** (1999) 125-130, doi:10.1016/S0168-9002(99)00090-X.